Biological complexity facilitates tuning of the neuronal parameter space

*Marius Schneider[a,b,c,d], Alexander D Bird[a,b,c] Albert Gidon[e], Jochen Triesch[a,d,f], Peter Jedlicka[a,c,g,1], *Hermann Cuntz[a,b,1]

[a]Frankfurt Institute for Advanced Studies, 60438 Frankfurt am Main, Germany
[b]Ernst Strüngmann Institute (ESI) for Neuroscience in cooperation with the Max Planck Society, 60528 Frankfurt am Main, Germany
[c]ICAR3R – Interdisciplinary Centre for 3Rs in Animal Research, Justus Liebig University Giessen, 35390 Giessen, Germany
[d]Faculty of Physics, Goethe University, Frankfurt/Main, 60438 Frankfurt am Main, Germany
[e]Institute for Biology, Humboldt-Universität zu Berlin, Berlin, Germany
[f]Faculty of Computer Science and Mathematics, Goethe University, 60438 Frankfurt am Main, Germany
[g]Institute of Clinical Neuroanatomy, Neuroscience Center, Goethe University, 60528 Frankfurt am Main, Germany

[1]Joint senior authors

*marius.schneider@esi-frankfurt.de, cuntz@fias.uni-frankfurt.de

Keywords

Dendrite function, Degeneracy, Electrophysiology, Compartmental modelling, Evolutionary principles, Law of large numbers

In brief

Studying ion channel diversity in neuronal models we show how robust biological systems may evolve not despite but because of their complexity.

Highlights

- 15 channel model of hippocampal granule cells (GCs) reduces to 5 ion channels without loss of spiking behaviour.
- But knocking out ion channels can be compensated only in the full model.
- Random sampling leads to $\sim 6\%$ solutions in full but only $\sim 1\%$ in reduced model.
- Law of large numbers generalises our observations to other complex biological systems.

Abstract

The electrical and computational properties of neurons in our brains are determined by a rich repertoire of membrane-spanning ion channels and elaborate dendritic trees. However, the precise reason for this inherent complexity remains unknown. Here, we generated large stochastic populations of biophysically realistic hippocampal granule cell models comparing those with all 15 ion channels to their reduced but functional counterparts containing only 5 ion channels. Strikingly, valid parameter combinations in the full models were more frequent and more stable in the face of perturbations to channel expression levels. Scaling up the numbers of ion channels artificially in the reduced models recovered these advantages confirming the key contribution of the actual number of ion channel types. We conclude that the diversity of ion channels gives a neuron greater flexibility and robustness to achieve target excitability.

Significance statement

Over the course of billions of years, evolution has led to a wide variety of biological systems. The emergence of the more complex among these seems surprising in the light of the high demands of searching for viable solutions in a correspondingly high-dimensional parameter space. In realistic neuron models with their inherently complex ion channel composition, we find a surprisingly large number of viable solutions when selecting parameters randomly. This effect is strongly reduced in models with fewer ion channel types but is recovered when inserting additional artificial ion channels. Because concepts from probability theory provide a plausible explanation for this improved distribution of valid model parameters, we propose that this may generalise to evolutionary selection in other complex biological systems.

Introduction

Throughout evolution, biological cells have emerged with increasing diversity and complexity. Optimising for multiple objectives while keeping an ever larger number of cell parameters within a viable range seems a daunting task for evolutionary processes; and it remains unclear how such a multi-objective optimisation can be achieved in the corresponding high dimensional parameter space. Here we explore the counter-intuitive hypothesis that increasing the number of mechanisms – i.e. increasing the biological complexity – potentially helps systems to evolve more quickly, easily and efficiently towards satisfying a large number of objectives.

Neurons are a good example of complex cells, typically exhibiting a great diversity in the expression of ion channels as products of such evolutionary optimisation. The channel parameters must be tuned to cooperatively generate multiple features of neuronal spiking behaviour. A palette of such spiking features has been successfully used in computational biophysical neuron models for multi-objective optimisation (MOO) using genetic algorithms (Druckmann, 2007). Mammalian neurons contain a large variety of ion channels types in their membrane (Coetzee *et al.*, 2006) producing a wide range of possible spiking mechanisms with varying temporal dynamics and excitability (Connors and Gutnick, 1990). Interestingly, a number of these ion channel variants exhibit overlapping functional properties (Coetzee *et al.*, 2006; Rudy, 1988; Herrera-Valdez *et al.*, 2013; Marder and Goaillard, 2006; Olypher and Calabrese, 2007; Hille, 2001; Goaillard and Marder, 2021). A large body of literature has explored the reason for this high diversity (Marder, 2011; Prinz *et al.*, 2004; Golowasch *et al.*, 2002; O'Leary *et al.*, 2013). However, it remains unclear what role exactly the diversity of ion channel types plays regarding evolution and its contribution to functional mechanisms that impact neuronal computations.

Neuronal computation relies on the morphology as well as on the diversity and distribution of ion channels in the membrane of the dendritic tree, the soma, and

the axon initial segment. Even small changes in the distribution of ion channels can change the activity in neurons drastically (Achard and De Schutter, 2006). Large differences in experimental measurements have been observed from cell to cell, day to day and animal to animal in data from the same classes of cells (Marder and Goaillard, 2006; Golowasch *et al.*, 2002; Golowasch and Marder, 1992; MacLean *et al.*, 2003; Swensen, 2005; Schulz *et al.*, 2006, 2007). The expression levels of these ion channel types can vary several-fold across neurons of a defined type (Marder and Goaillard, 2006; Prinz *et al.*, 2004; Golowasch *et al.*, 2002; Golowasch and Marder, 1992; MacLean *et al.*, 2003; Schulz *et al.*, 2006). However, many detailed biophysical models of single cells ignore this variability in electrophysiological data and search for a fixed set of parameters that replicates an average behaviour of a particular cell type (Golowasch *et al.*, 2002).

How can neurons manage to achieve a functional target activity with such a wide ion channel diversity? Using a spike-feature-based multi-objective approach, we generated large population parameter sets of dentate granule cell (GC) models with different numbers of ion channel types in order to investigate the potential advantages of ion channel diversity. We then tested to which degree the different models could compensate for pathological channel loss. Furthermore, we investigated differences in functional parameter sets, taking into account stochastic fluctuations in channel-coding gene expression. Finally, we studied the stability of the different models against ion channel alterations due to e.g. protein turnover. We found that in all cases the complete GC model with all ion channel types was more robust, stable and had more valid parameter combinations than its reduced counterparts.

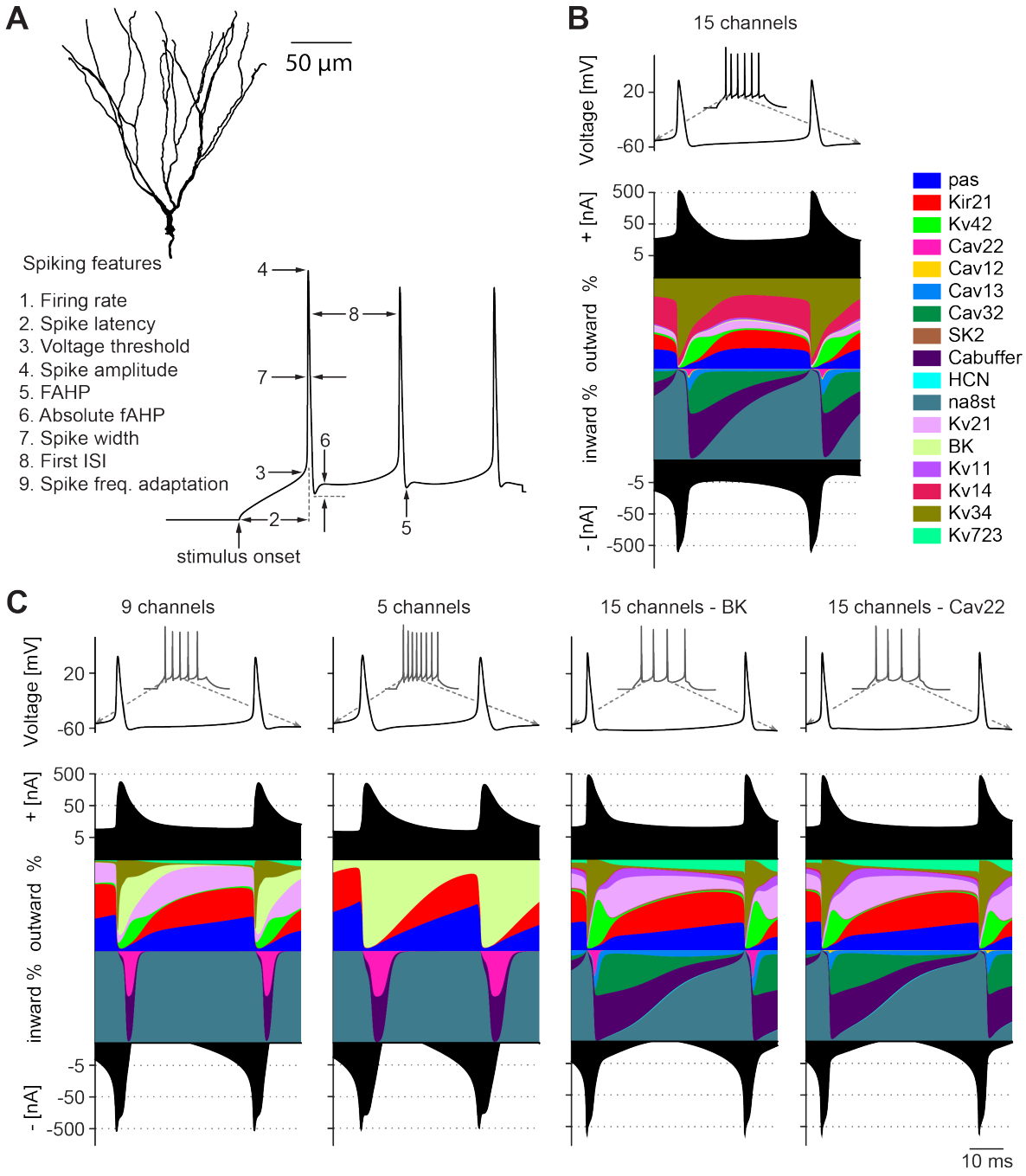

Figure 1. Simplified as well as realistic complex ion conductance-based models capture multiple spiking features of real granule cells (GCs)

A, (*Top*) 3D-reconstructed mouse GC morphology used for our simulations (Schmidt-Hieber *et al.*, 2007). (*Bottom*) Spike features used to calculate the multi-objective fitness of the GC model. **B**, Membrane potential during $200ms$ lasting current clamp of $90pA$. The coloured curves show the relative contribution of all implemented ion channels to the total inward (See next page)

Figure 1. (continued) and outward current at each time step (during the second and third spike) as a percentage of the total current. The black filled curves illustrate the total inward and outward currents on a logarithmic scale. This plot was inspired by Alonso and Marder (2019).**C**, Contribution of currents to total inward and outward current in reduced models and models that compensate for the knock out of the BK (*Left*) and Cav22 (*Right*) channel. Similar visualisation and current injection procedure as in **B**.

Results

We used a recently established multi-compartmental model comprising the 15 different voltage or calcium-dependent ion channels that were described in mouse GCs (Beining *et al.*, 2017). The model was specifically designed to reproduce the results not of a single experiment but of a large series of experiments and was based on raw electrophysiology traces. Its parameters were fitted to reproduce the experimental data for a number of different reconstructed (see example in **Figure 1A**, *Top*, from Schmidt-Hieber *et al.*, 2007) and synthetic neuronal morphologies making the model robust within the GC morphological space. Furthermore, the resulting model readily generalised to rat GCs as well as to adult born mouse GCs (i.e. GCs from adult mouse neurogenesis) after incorporating the known changes in morphology and ion channel composition. The model can therefore be considered to be robust and comprehensive. This makes it an experimentally validated tool to study the impact of complex ion channel compositions on robustness of the spiking output. To this end, we employed a population (also called "ensemble" or "database") modelling approach, which allowed us to explore the multidimensional parameter space in large populations of stochastically generated models (Prinz *et al.*, 2003; Gunay *et al.*, 2008; Britton *et al.*, 2013; Sekulic *et al.*, 2014; Rathour and Narayanan, 2019; Jedlicka *et al.*, 2022).

The GC model cost function

First, we developed a cost function for an automated evaluation of the validity of diverse models, which differed in their ion channel combinations and densities. Since no quantitative data exists on the particular expression of the various ion channels in individual GCs, some form of fitting procedure of channel densities was required in the construction of the GC model. The model consists of 27 conductance parameters, which precludes a comprehensive grid scan for parameter fitting due to the long computing time in a 27 dimensional parameter space. The model has therefore previously been largely tuned manually with expert knowledge from GC biology. To assess the quality of any individual set of parameters more automatically, we designed a fitness function that quantified the distance to experimental spiking data and was inspired by approaches used previously (Druckmann, 2007; Beining *et al.*, 2017, see Methods, **Figure S1**). A number of different methods have been proposed to quantify the quality of a set of parameters in relation to neuronal activity (Achard and De Schutter, 2006; Bahl *et al.*, 2012; Keren *et al.*, 2005; Vanier and Bower, 1999). While most studies focus on reproducing an average electrophysiological activity pattern, we wanted to focus on the distribution of valid parameter combinations in the GC model taking into account the variability present in experimental data.

We therefore used a multi-objective fitness function based on spike features, which allowed us to search for optimal trade-offs between different firing properties (Druckmann, 2007). We extracted 9 different spiking features from raw electrophysiology traces during a $200ms$ current clamp injection with 50 and $90pA$ at the soma (**Figure 1A**, *Bottom*, see Methods). We then compared the values for these features between the model and the experimental data. To generate a population of GC model instances that reflected the full range of firing properties, we calculated the deviation from the experimental mean in units of experimental standard deviation (SD) (Druckmann, 2007). In order to become a valid parameter combination in the GC model, the error value was required to be less than two SDs away from the

experimental average of each feature.

A manual search for parameter sets fulfilling this requirement was very time-consuming and could never be exhaustive. There are various automated parameter search methods, such as gradient descent methods, genetic algorithms, simulated annealing, and stochastic search methods, which make the search for parameters more efficient (Vanier and Bower, 1999; Mitchell, 1998; Kirkpatrick *et al.*, 1983; Press *et al.*, 2007). Since we were starting from a valid parameter combination, we decided to use a gradient descent algorithm (Press *et al.*, 2007) in combination with random parameter space exploration (see Methods). This method also led to good parameter combinations within a few iteration steps when starting from random parameter sets for which the model deviated from the experimental results. By combining random parameter exploration with a gradient descent method, parameter combinations could even be found when starting from initial parameter sets for which the models produced no spikes at all (**Figure S2**).

Reduction of channel diversity

Electrophysiological signatures of neurons of the same class are often unique allowing a loose classification of cell types by their electrophysiology. However, the spiking mechanisms often include multiple ion channels with overlapping functionality to achieve these specific spiking behaviours (Coetzee *et al.*, 2006; Olypher and Calabrese, 2007; Marder, 2011; Bean, 2007; O'Leary *et al.*, 2014; Drion *et al.*, 2015; Goaillard and Marder, 2021). Thus, an important question is, how many channels are functionally necessary for a given cell type. We addressed this question in GCs whose membrane contains a large palette of voltage- and calcium-dependent conductances (Beining *et al.*, 2017). The compact activity together with the multitude of ion channels in the corresponding GC model (**Figure 1C**) suggests that a reduction of channels without losing accurate model performance might be possible. Therefore, we explored this possibility by incremental simplification of the GC model. First, we reduced the number of voltage-dependent conductances

in the highly detailed multi-compartmental model of GCs by 6 channels (removing Cav12, Cav13, Cav32, Kv11, Kv14, SK, **Figure 1C**, *Leftmost*). This left a total of 13 parameters when expression in the different regions of the neuron are taken into account. Thereupon, we gradually reduced the number of remaining channels to a minimum of 5 ion channels (9 total parameters, leaving only the leak channels pas, as well as Kir21, Na8st, BK and Cav22) finding parameter combinations that satisfied our cost function using the search algorithm (**Figure 1C**, *Center left*).

To visualise the contribution of individual currents to neuronal model activity, we employed a recently developed method of plotting the time course of the relative contribution of each ionic current (Alonso and Marder, 2019). Overall, as expected, the electrophysiological activity of the different valid models in **Figure 1C** was similar (for overview, see **Figure S3**). Despite the large variations in the number of ion channels, the course of the total inward and outward current flow displayed only slight changes between the three different baseline models (**Figure 1B, C**). Since GCs have a relatively simple electrophysiological repertoire (nevertheless responsible for sophisticated integration of excitatory and inhibitory information), a small number of membrane time constants was sufficient to generate adequate firing patterns. The presence of K^+ and Ca^{2+} channels with overlapping physiological functionality ensured that many of the channels were not crucial for the maintenance of functional activity. Only the composition of the inward and outward currents differed. In the $5-$channel model, the calcium-sensitive potassium channel (BK) took over the role that 8 different K^+ conductances had shared in the non-reduced model (**Figure 1C**). BK thereby became the only remaining K^+ channel overall. In interaction with the Ca^{2+} conductances (Cav22), the BK channel was responsible for repolarising the membrane potential following an action potential in the $5-$channel model.

Recent experimental and theoretical studies demonstrated that neurons can compensate for pathological changes such as channel loss, genetic overexpression, morphological changes or increased input activity by up- and downregulation of the remaining ion channels (Guo *et al.*, 2005; Nerbonne *et al.*, 2008; Aizenman *et al.*,

2003; Turrigiano *et al.*, 1999; O'Leary *et al.*, 2010; Young *et al.*, 2009; Stegen *et al.*, 2012). This ability should be impaired in the reduced model where less redundancy exists. Indeed, we found that blocking the BK or N-type Cav22 channels in the full model was readily rescued by contributions from other channels (**Figures 1C**, *Right*). It is noticeable that the loss of the BK channel was compensated by a strong upregulation of another calcium-sensitive channel (SK), as well as of voltage-dependent potassium channels (Kv 7.2/3, Kv 1.1, Kv 2.1, **Figure S4**, *Left*). Neither loss of BK nor Cav22 could be compensated for in the reduced $5-$channel model since it had only one active gating mechanism per ion type. Even the $9-$channel model was not able to compensate for the pathological loss of Cav22 or BK. As expected, therefore, the full GC model's diversity contributed to the model's robustness with respect to the loss of specific ion channels through existing ion channel redundancies.

Random parameter tuning as a viable approach to selecting GC model

Even though small changes in the ion channel expression level can already lead to drastic changes in neuronal activity, several experimental studies observed that intrinsic properties of nerve cells can vary considerably across neurons of the same type (Golowasch *et al.*, 2002; Golowasch and Marder, 1992; MacLean *et al.*, 2003; Swensen, 2005; Schulz *et al.*, 2006, 2007). Moreover, theoretical investigations demonstrated that indistinguishable network and single neuron activity can be obtained from a large variety of model parameter settings (Prinz *et al.*, 2004; Golowasch *et al.*, 2002). This raises the question of whether the diversity of voltage- and calcium-dependent conductances has an effect on the variability of valid parameter sets in the GC model leading to realistic spiking activity.

In order to check this, we first generated $20,000$ random model instances for each of the three baseline models by randomly sampling the individual conductance densities within a range between $0\times$ and $2\times$ the value in the baseline model. As

the ohmic relations between current and voltage were consistent with experimental results in all cases (see **Figure S3B**), we did not change the densities of the leak channel or the inward-rectifying Kir21 channel, which primarily contribute to the passive properties of the neuron. The population of functional parameter combinations enabled us to calculate the Pearson's correlation coefficient r for all pairs of conductance density parameters. We found weak pairwise correlations indicating low dependencies between each pair of channels and thus increasing the robustness of the model (**Figure S5**). It is likely that higher-order correlations are more prevalent in the higher-dimensional models, allowing for more different solutions that compensate for fluctuations in the expression of a single channel. The strongest pairwise correlation was observed between the expression levels of the Na^+ channel in the soma and in the AIS ($r = -0.95$). The sodium channel is essential for spike initiation and its presence in different regions of the GC suggests that compensatory mechanisms could simply be instantiated by maintaining a balance between the same currents in different regions, which results in a significant anticorrelation. Interestingly, the reduced models showed stronger and different correlations between the channels than the full model.

In our selection of random parameter combinations, we found suitable models covering the entire sample range of the majority of parameters (**Figure 2**). In all cases, the most constrained parameter was the density of the $8-$state Na^+ channel. This channel models the behaviour of all Na^+ conductances using a single maximum conductance parameter (Schmidt-Hieber *et al.*, 2007), so it is unsurprising that the neuron's behaviour is more sensitive to changes in this maximum. In addition, the reduction of channel diversity in the $5-$channel model limited the variability of the calcium-dependent potassium channel BK (**Figure 2**, *Right*). Surprisingly, the overall percentage of randomly selected parameter combinations that were valid increased with the number of ion channels (**Figures 3A, B**, $\sim 0.7\%$ with 5 channels (for 9 total parameters), $\sim 3.3\%$ with 9 channels (13 parameters), and $\sim 5.7\%$ with 15 channels (27 parameters)).

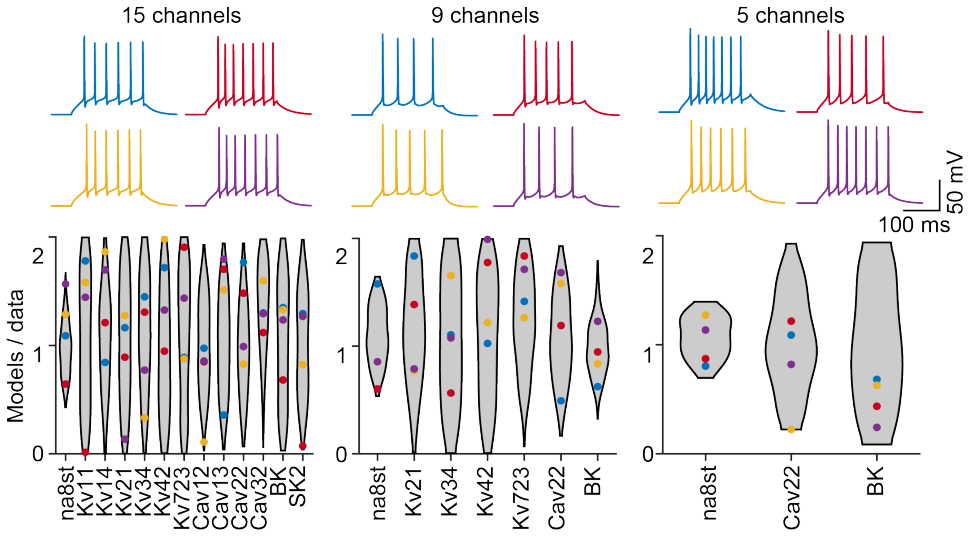

Figure 2. Valid parameter combinations in the fully complex model are well spread.
(*Top*) Activity traces of 4 randomly picked valid parameter combinations in each of the GC models of different complexity. (*Bottom*) Coloured dots illustrate conductance densities of the four valid parameter combinations shown in top traces. The grey violin plots delimit the entire range covered by the valid parameter combinations. Conductances are weighted by the surface area of the corresponding membrane regions.

The distribution of voltage- and calcium-activated channels in cell membranes is under continuous regulation (Raj and van Oudenaarden, 2008; Gal *et al.*, 2010; Marder *et al.*, 2014). On the one hand, the cell is subject to homeostatic regulation maintaining its electrical activity despite changes in its environment and input. On the other hand, the proteins are constantly exchanged during the lifetime of a cell. In order to investigate the stability of the valid parameter combinations in the different models in face of parameter perturbations due to e.g. protein exchange during the lifetime of a cell, we performed random walks in the parameter space. Starting from a valid parameter set that accurately reproduced the experimentally derived behaviour, we iteratively changed each parameter by random steps between -5% and $+5\%$ of the current parameter values (counting changes in all parameters as one step). The random walk stopped as soon as the parameter combination became invalid, i.e. the cost function for the resulting model increased beyond 2 standard

deviations away from experimental results. Interestingly, the average number of possible random parameter changes before model failure increased with the number of ion channels in the models (**Figure 3C**).

Toy model points to law of large numbers

As shown in the previous sections, we observed an increase in valid random parameter sets when biophysical models of neurons became more complex. One possible explanation could be the fact that the more complex models included different ion channels of a similar type. Since some of these ion channels show very similar gating dynamics (see for example Cav22, Ca12 and Cav13, see **Figure 1**) their functional contributions may be partially redundant. A theorem from probability theory, namely the law of large numbers can play a role under such circumstances. The law of large numbers states that increasing the number of samples (in our case ion channels of a similar type) described by a random variable will move the average over the samples closer to the expected mean value. For example, throwing multiple fair dice with sides numbered between 1 and 6 and adding the results will tend to give a result that is relatively closer to the expected value (the number of dice multiplied by 3.5) as more dice are used. Since in our case we sample conductances of similar ion channels, the average conductance would therefore converge towards the starting parameter set that we know is functional.

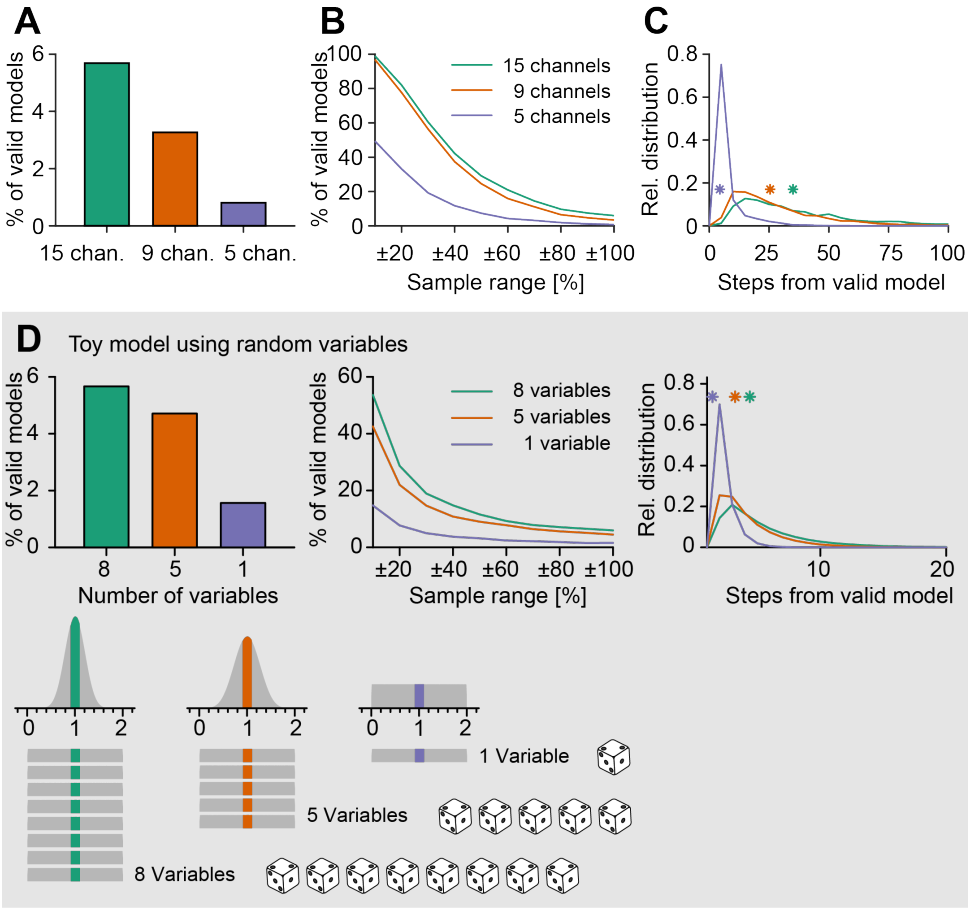

Figure 3. Valid parameter combinations in the fully complex model are more stable as compared to reduced models.

A, Percentage of valid random parameter combinations in the total population in the $2-$fold range. **B**, Percentage of valid random parameter combinations in samples with different ranges around the valid reference parameter combination. Each sample contained $5,000$ parameter combinations. **C**, Random walk through the parameter space starting from valid combinations in models of different complexity. Relative percentage distribution of the maximum number of random steps the respective models could undergo without losing their valid GC spiking behaviour. Bin size is 4 steps. Asterisks indicate mean number of steps the corresponding models could undergo while maintaining realistic activity. Performed for $2,000$ repetitions per model. **A–C**, Colours were Green: full model, Orange: $9-$channel model, Purple: $5-$channel model. **D**, Reproduction of **A–C** with a toy model representing the model result as the average value of 1 (blue), 5 (red) and 8 (green) uniform random variables between 0 and 2. *Bottom panels*, Illustration of how the distribution of solutions becomes narrower when the number of variables is increased. This effect is explained by the law of large numbers while the Gaussian distribution results from the central limit theorem.

In order to illustrate this we designed a simple toy model using random variables for each parameter. Here, we represented each open parameter of the model by one random variable with a homogeneous probability of throwing any number between 0 and 2 corresponding to the parameter ranges used in the neuronal model between $0\times$ and $2\times$ the default value (**Figure 3D**, *Bottommost*). To keep things simple for explanatory purposes, we set the model outcome to be the statistical mean of the values of all separate random variables. The law of large numbers predicts a decreasing variance of the mean value with an increasing number of independent random variables as illustrated in the sketch at the bottom of **Figure 3D**. The central limit theorem in turn predicts a Gaussian distribution for this mean over a broad range of different probability distributions for each random variable separately. In analogy to our neuronal modelling, we then constrained valid parameter combinations by a cost function allowing a maximal distance of 0.015 from the mean value, i.e. 1, averaged over all random variables.

The analogy here is limited since, in contrast to the channels in the GC model, all variables in our toy model are functionally the same and independently regulated. Moreover, the GC compartmental model applies complex nonlinear and dynamic transformations of the starting parameter space, including distinct jumps in the cost function when the model no longer produces action potentials, to reach the cost (or function) space; in the toy model the parameter and function spaces are effectively indistinguishable. However, despite its simplicity, our toy model was able to qualitatively reproduce all results from our GC model in **Figure 3A–C** (**Figure 3D**). Adding correlations to the parameter space does not qualitatively change the results (**Figure S6A**). An important observation here is that the constraint on functionality implies negative correlations between the values of the individual random variables that make up valid points in the parameter space, despite these variables being generated independently or with positive correlations. In fact, under the toy model framework, the pairwise correlations within variables that produce valid models are almost completely independent of any correlations used to generate the overall population from which valid models are drawn (**Figure S6B**).

The output correlations are instead dependent on the number of variables, with higher numbers of variables leading to weaker pairwise correlations. This result agrees with the finding of stronger pairwise correlations between channel densities in the 5-channel model compared to the full compartmental model (**Figure S5**).

The law of large numbers therefore provides a plausible explanation why a larger number of random instances in the more complex neuron model would more readily linger around their target functionality.

Additional model robustness through artificial ion channel isoforms

We have shown that the electrophysiological behaviour of GCs can be maintained despite a reduction of ion channel diversity from 15 channels to 5 channels. However, our results also suggest that this loss of ion channels goes along with a decrease in stability, a loss of compensatory opportunities, and a significant decrease in the valid model percentage within a randomised sample. From our toy model based on probability theory we postulate that it might be the mere number of ion channels that contribute to the increased robustness observed in the full model rather than the particular ion channel composition present there. In order to validate this hypothesis, we chose to start from the reduced model and increase the number of ion channels in an artificial way to check whether we could recover the robustness present in the realistic full model.

In order to establish a quantitative relation between channel diversity and model stability in such a way, we scaled up the $5-$channel model's diversity by adding more instances of the calcium (Cav22) and potassium channels (BK) remaining in that model. These artificial isoforms of the existing ion channels distinguished themselves from the original Cav22 and BK by randomised time constants (within a two-fold range of the original parameters) to allow for different dynamics through the new ion channel isoforms.

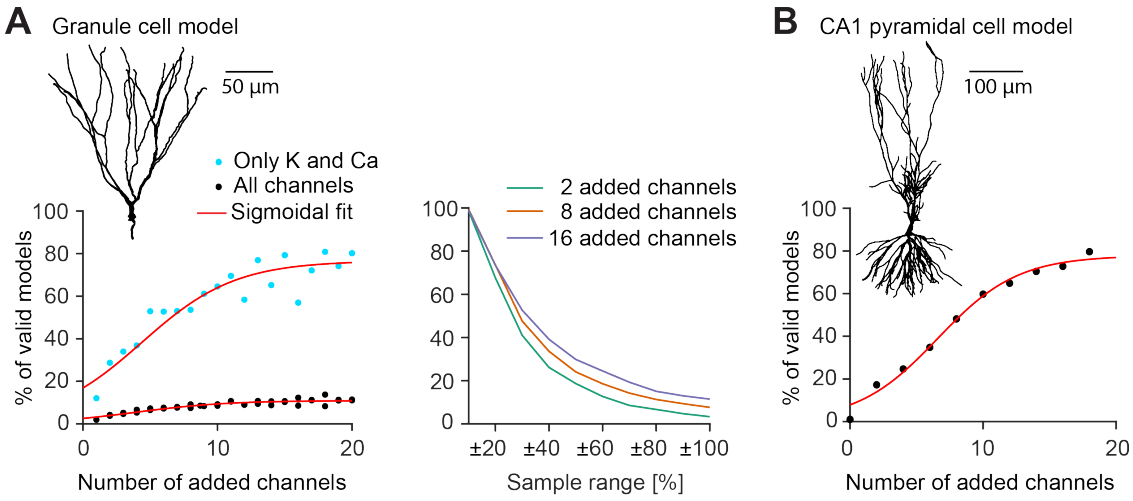

Figure 4. Artificial expansion of ion channel diversity recovers and enhances the proportion of valid parameter combinations in the reduced 5-channel model

A, Populations of expanded dentate GC models with $0-20$ added artificial ion channel isoforms. *Left panel*, The plot shows the percentage of functional parameter combinations in a population of randomly sampled channel densities. Black dots show the populations where all ion channels (including the $8-$state Markov chain modelled Na^+ channel) were sampled in a $0-2\times$ range. Blue dots show the populations where only potassium and calcium channels were sampled in a $0-2\times$ range. *Right panel*, Similar plot as in **Figure 3B** for the black models from the *left panel*. **B**, Similar overall analysis as in **A** but for a CA1 pyramidal cell model (Jarsky *et al.*, 2005).

To examine the proportion of valid parameter combinations with increasing number of ion channels, we created a multitude of functional GC models with up to 20 additional ion channel isoforms (for 35 distinct channels in total). For each given number of ion channel isoforms, we randomly sampled all conductance values in a two fold range. Thereupon we selected the three parameter combinations with the best fitness value for each number of ion channel isoforms and improved their performance by applying a gradient descent algorithm. We then followed the same procedure as in **Figure 3**. Using this approach, the percentage of valid parameter combinations steadily increased with the number of additional ion channel isoforms until reaching a plateau between 15 and 20 additional ion channel isoforms, for a total of 105 to 140 additional parameters (**Figure 4A**). To further generalise our findings in **Figure 4A** we have applied the same procedure to a

different neuronal model type, one simulating a CA1 pyramidal neuron (Jarsky *et al.*, 2005; Cuntz *et al.*, 2021, **Figure 4B**). Viewed together, these results show the major contribution of ion channel diversity by demonstrating that scaling up the numbers of ion channels artificially in the reduced models leads to more frequent valid parameter combinations. This is in line with the law of large numbers.

Discussion

In this study, we explored the complex landscape of valid parameter combinations in a parameter space of a detailed multi-compartmental model of dentate GCs and its simplified versions with reduced numbers of ion channels (**Figure 1**). We used a population modelling approach (Gunay *et al.*, 2008; Marder, 2011; Britton *et al.*, 2013; Sekulic *et al.*, 2014) to find multiple ion channel parameter combinations for models that successfully reproduced the electrophysiological data (**Figures 2 and S1**). We show that the biologically realistic GC model (full model) with many redundant ion channel types was more robust to ion channel perturbations than valid models with reduced ion channel diversity. Importantly, noisy ion channel expression simulated by random parameter combinations produced $\sim 6\times$ more valid GC model instances in the full model as compared to the reduced models (**Figure 3**). The robustness in the reduced model was recovered when adding artificial isoforms of existing ion channels (**Figure 4**) indicating that it is indeed the number of channels that produces this effect. We argue that this increased robustness comes in part from a direct consequence of basic probability theory.

Robustness through ion channel degeneracy in complex GC models

Most neurons contain more than a dozen different ion channels. While early computational models implemented considerably fewer channels than known in biology, more and more models exist that contain a realistic number of mechanisms

(e.g. Beining *et al.*, 2017; Hay *et al.*, 2011). Although the different potassium channels in mammalian cortical neurons differ genetically, some are remarkably similar in their functional contribution to the electrophysiological activity of neurons (Coetzee *et al.*, 2006; Drion *et al.*, 2015). This functional similarity is often referred to as degeneracy (Goaillard and Marder, 2021) and is not a phenomenon restricted to neurobiology (Edelman and Gally, 2001; Tononi *et al.*, 2002). Depending on the computations a neuron should implement, its dynamics only need to cover certain relevant time scales, e.g. in the form of different time constants of its gating variables (Gjorgjieva *et al.*, 2016). Since five channels were sufficient to support realistic voltage dynamics at relevant time scales, we were able to reduce the original variety of ion channels without observing a significant loss in the performance of the model. In our study, GCs with their compact electrophysiological repertoire did not require a large variety of ion channels to reproduce their characteristic activity patterns. To replicate the 9 experimentally derived spiking properties, the models required only one active channel of each of the different subgroups of ion channels (one Na^+-, one K^+- and one Ca^{2+}-channel, as well as the leak channels; **Figure 1C**).

Experimental as well as theoretical studies from the last decades revealed that pharmacological manipulations like the blockage or upregulation of intrinsic or synaptic mechanisms, resulting in a pathological cellular activity on a short timescale, can be compensated by up- and downregulation of the remaining conductances on a long timescale (MacLean *et al.*, 2003; Swensen, 2005; O'Leary *et al.*, 2014; Drion *et al.*, 2015; Guo *et al.*, 2005; Nerbonne *et al.*, 2008; Stegen *et al.*, 2012; MacLean *et al.*, 2005). Interestingly, not all manipulations can be compensated by mechanisms of homeostatic regulation (Zhang *et al.*, 2003; Yang *et al.*, 2022), indicating differences in the capability of homeostatic compensation between ion channels as well as types of neurons. As opposed to other studies using biophysically realistic mechanisms of homeostatic intrinsic plasticity based on calcium signals (O'Leary *et al.*, 2013, 2014; Abbott and LeMasson, 1993; Golowasch *et al.*, 1999; Liu *et al.*, 1998; Franci *et al.*, 2020; see also Yang *et al.*, 2022), we decided to use a gradient

descent approach to investigate the large and complex parameter space of possible intrinsic compensations. We chose this mathematical approach also because the biophysical mechanisms of intrinsic plasticity are not yet fully understood in detail. The implementation of biophysically incomplete mechanisms of intrinsic plasticity could lead to unnecessary limitations on the regulatory mechanisms and erroneous conclusions. A homeostatic mechanism based on a single feedback signal (O'Leary *et al.*, 2013, 2014) that has been suggested to play a role in model robustness was not compatible with our model in our hands since it decreased ion channel degeneracy. This is in agreement with a recent study (Yang *et al.*, 2022) that provided new insights into the complex relationship between ion channel diversity and homeostatic co-regulation of ion channel densities. The study by Yang *et al.* (2022) suggested the necessity of more than one master feedback regulator (i.e. more regulators than just global calcium) for homeostatic feedback loops, which must co-tune numerous degenerate and pleiotropic ion channels to achieve multiple regulated functions or objectives (cf. Pallasdies *et al.*, 2021; Jedlicka *et al.*, 2022). Viewed together, we believe that diversity and (multi-signal) feedback can act as independent mechanisms to ensure viable and robust solutions to multi-objective optimisation problems of neurons.

We demonstrated that the full GC model was capable of compensating the loss of any potassium and calcium channels by up- and downregulation of the remaining ion channels (**Figure 1C**). In contrast, the different reduced models relied on the presence of certain indispensable ion channels, without which they could not capture main electrophysiological characteristics of GCs. **Figure S4** shows that there can be as much as a $20-$fold variability in the density of voltage-dependent ion channels. Experimental studies have observed variations of a similar order of magnitude as a result of compensatory mechanisms (MacLean *et al.*, 2003). The ability of these models to compensate for losses of ion channels can be attributed to the overlapping or degenerate physiological function of the present potassium and calcium channels (Mishra and Narayanan, 2021).

The reduction of the diversity of gating mechanisms goes along with a loss of space

to manoeuvre in the process of achieving functional target activity (O'Leary *et al.*, 2013; Drion *et al.*, 2015). In case of a loss of the BK channel, several potassium channels (see **Figure S4**) were upregulated, and thus maintained the functional behaviour of the cell. In line with the concept of degeneracy (Druckmann, 2007; Aizenman *et al.*, 2003), the overlapping functionality of different channels enabled the neuron, depending on the given conditions, to achieve a target spiking behaviour in a number of different ways.

In addition, we tested the stability of the differently reduced models against random parameter perturbations, in order to simulate putative protein exchange during the lifetime of a cell. The ongoing protein replacement is one of the reasons for the continuous regulation of voltage- and calcium-dependent channels in cell membranes (Raj and van Oudenaarden, 2008; O'Leary *et al.*, 2014; Gal *et al.*, 2010). Although no homeostatic tuning mechanism with dynamic feedback was implemented, valid parameter combinations in the complete model were able to endure far more random parameter perturbations while maintaining realistic activity than the ones in the reduced models (**Figure 3C**). This is in agreement with experimental studies, which have shown that, although homeostatic tuning rules can compensate for many perturbations and knock-outs of ion channels, not all channel deletions and perturbations can be compensated for (Zhang *et al.*, 2003). A challenge for future experimental work will be to uncover the long-term effects of ion channel knock-outs in GCs in order to find out whether our theoretical results of the outstanding robustness of GCs against channel deletions can be observed in biology.

Random parameter selection as a viable fitting strategy for neurons

Like many biological processes, gene expression is a largely stochastic process resulting in considerable heterogeneity of mRNA and protein levels (Raj and van Oudenaarden, 2008; Gal *et al.*, 2010; Sigal *et al.*, 2006). This noise in gene expression is one reason for the cell-to-cell variability. However, noise in gene expression

could be harmful for achieving functional parameter sets of ion channel expression during developmental maturation or during pathological perturbations. Neurons are thought to target certain desired set points (or set ranges) in the output space (i.e. function or behaviour space) corresponding to valid points or subspaces in the high-dimensional parameter space of expression levels of ion channels (Jedlicka *et al.*, 2022). Our simulations show that the subspace around these target values in parameter space tends to be more densely filled with functional model parameters than non-valid parameters (**Figure 3B**), particularly in higher dimensions. Accordingly, despite fluctuations, high-dimensional models are more likely to end up in functional subspaces. Even without the implementation of homeostatic regulation processes, the chance of obtaining a functional ion channel expression level is relatively high. This implies that the degeneracy between ion channel types and isoforms supports robust excitability profiles in neurons despite random fluctuations in the expression of ion channels. Our computational analysis indicates that a complex high-dimensional parameter space supports the stability of neuronal excitability against perturbations that would push neurons into non-functional subspaces. The reason is that the topology of the high-dimensional space increases the likelihood of neurons returning into functional subspaces by random ion channel parameter adjustments. An interesting extension would be to compare the efficiency of activity-dependent regulation (O'Leary *et al.*, 2014; Franci *et al.*, 2020; Yang *et al.*, 2022) implemented with single or multiple homeostatic error signals (Yang *et al.*, 2022), with the multi-objective optimisation (Druckmann, 2007; Van Geit *et al.*, 2008; Pallasdies *et al.*, 2021; Jedlicka *et al.*, 2022) that arises naturally from stochastically exploring high-dimensional parameter spaces.

Due to the diversity of electrophysiological mechanisms, the cell is able to generate valid electrophysiological activity by random selection of parameters with a high chance of success despite stochastic fluctuations in the expression of channel-coding genes. We showed that there was a clear relation between the number of intrinsic mechanisms and the chance to obtain a valid set of parameters from a random sample around a valid point in parameter space that produces functional

activity in output space (**Figures 3A, B, and 4**). Furthermore, we showed that many other parameter combinations existed around such a functional point in the parameter space that fulfilled our criteria for functional activity. While in a random $0 - 2\times$ fold sample of the initial model, about $\sim 5.7\%$ of the parameter combinations showed valid GC activity, this proportion decreased steadily to $\sim 0.7\%$ with a reduction of the model (**Figure 3A**). In the closer surrounding of the baseline models this difference was even more obvious. While in the unreduced model in the close neighbourhood of $\pm 20\%$ of the initial parameter sets over 80% of the models showed characteristic GC activity, in the heavily reduced model it was only about 30% (**Figure 3B**).

Similar to Olypher and Calabrese (2007) and Achard and De Schutter (2006) we showed that near each functional point in the parameter space many other parameter sets exist whose activity matches the activity of the original parameter set (**Figure S7 – S9**). Instead of talking about parameter sets, one might rather speak about subspaces that show functional behaviour. These subspaces can have different densities of parameter sets showing characteristic electrophysiological activity. This depends to a great extent on the diversity of the channels (**Figures 3A, B, and 4A, *Left panel***). Furthermore, different valid subspaces with the same diversity differ in their density of functional solutions located in this subspace. In order to be as robust as possible against perturbations and to simplify the process of parameter fitting, it seems reasonable for a neuron to target as densely populated a subspace as possible.

Ion channel correlations and random expression

When analysing the conductance values of the different types of ion channels in the valid models, we observed that some pairs of ion channels shared significant correlations (**Figure S5**, *Red squares*). This is in line with experimental studies of cell-to-cell variations in ion channels showing that some ion channels are co-expressed and might be co-regulated (Schulz *et al.*, 2006, 2007; Khorkova and

Golowasch, 2007; Tapia *et al.*, 2018; Iacobas *et al.*, 2019; Fujita *et al.*, 2020; Kodama *et al.*, 2020). Future large-scale analysis of channel expression in real populations of GCs might validate the diversity of and correlations between expression levels in our population models.

In our simulations, the ion channel correlations arose from constraints on the resultant functionality because our model-generating strategy sampled the ion conductance levels independently. Although our population modelling was inspired by random noise in gene expression, it does not imply that random noise is the only or predominant source of cell-to-cell variability in ion channel expression. Since the above mentioned experimental studies found ion channel co-expression, it is likely that a great amount of the cell-to-cell variability in ion channel expression is due to transcription regulatory mechanisms, and only to some extent to the unreliable and noisy nature of gene expression mechanisms. Moreover, the widespread ion channel co-variations, which suggest structured ion channel expression in high-dimensional space, might arise potentially from homeostatic feedback mechanisms (O'Leary *et al.*, 2013, 2014; Franci *et al.*, 2020; Yang *et al.*, 2022; see above). These observations and models do not undermine our modelling strategy, but complement and extend our assumption that some of the variability in ion channel expression is due to intrinsic noise in the expression machinery.

Probabilistic toy model and law of large numbers

We have put forward the law of large numbers as a possible explanation for our observations in the GC model. As a consequence of the law of large numbers, a model containing more ion channels tends to exhibit a behaviour that is closer to its expected target behaviour (**Figure 3**). Accordingly, we were able to recover the amount of robustness observed in our full model when adding artificial ion channel isoforms (**Figure 4**). This is a strong indicator that indeed the number of ion channels and not their specific composition leads to the effect that we observed.

However, this interpretation is not mutually exclusive to the complementary insight from biophysical modelling that 15-channel model is more robust than the 5-channel one due to the increasing timescale and voltage coverage with the increasing number of ion channels (due to the partial, but not complete, redundancy between similar ion channels). The abstract toy model does not account for these two (time and voltage-related) mechanistic aspects but offers an intuition for the impact of the number of ion channel instances and their stochastic variation. The increase in the number of identical random variables in the toy model is analogous to the increase in the number of random instances of different ion channels. The main biological insight from the toy model is that if neuron samples conductances of similar ion channels around a functional point in parameter space, with the increasing number of channels the average conductance will converge towards the valid parameter set that produces functional behaviour. In summary, both biophysical and toy models indicate that the large number of ion channel subtypes and isoforms expressed by a neuronal type supports the tuning and robustness of the electrophysiological phenotype.

Conclusions and outlook

Overall, our results suggest that the diversity of ion channels allows for increased robustness and higher flexibility of finding a solution in the complex parameter space of a neuron's excitability. It will be interesting to investigate whether our findings here translate to other biologically complex systems, in which case they will most likely affect our general understanding of how evolution deals with complex organisms.

Acknowledgments

This work was supported by BMBF (No. 01GQ1406 - Bernstein Award 2013 to HC, No. 031L0229 - HUMANEUROMOD to PJ) and by funds from the von Behring Röntgen Foundation to PJ. JT acknowledges support by the Johanna Quandt foundation. MS was supported by the International Max Planck Research School (IMPRS) for Neural Circuits in Frankfurt. The authors declare to have no competing financial interests.

Author contributions

M.S., A.D.B., A.G., J.T., P.J., and H.C. designed the study. M.S. performed the simulations and analysed the data. M.S., A.D.B., A.G. J.T., P.J., and H.C. wrote the paper.

Materials and methods

All simulations were performed in *Matlab 2017b* (Mathworks, Natick, MA, USA). Single neuron simulations were performed using *T2N* (Beining *et al.*, 2017, `www.treestoolbox.org/T2N`), a Matlab interface between the open source package *TREES toolbox* (Cuntz *et al.*, 2010, 2011, `www.treestoolbox.org`) and the *NEURON* simulation environment (Hines and Carnevale, 1997, `www.neuron.yale.edu`). Predefined functions from *TREES toolbox*, *T2N* as well as additional custom *Matlab* code were used to generate and analyse the models. All code will be made available on Zenodo upon publication.

The granule cell (GC) model

The GC model used in this study has been fully described in (Beining *et al.*, 2017). Briefly, the model was designed to reproduce passive and active GC properties as determined by voltage and current clamp experiments, dendritic patch recordings of bAPs, and intracellular calcium imaging. In order to reduce the number of parameters and to speed up simulations we simplified the morphology by deleting the artificially added axon. The loss of the axon was compensated by slight changes of the maximum conductances in the axon initial segment (AIS). Since the HCN channel in its original form had no influence on control GC activity, we did not take it into account. The compartment-specific distributions of ion channels are shown in Table S1. Detailed descriptions of the individual ion channels can be found in Beining *et al.* (2017). We used a realistic three-dimensional granule cell morphology from Schmidt-Hieber *et al.* (2007).

Stimulation protocols and cost function

Instead of using a single optimal error function, we decided to adopt a strategy that allows to take into account several potentially important properties of GC activity. To get a first impression of the "goodness of a model", we compared the experimental (Mongiat *et al.*, 2009) and the model spiking-properties following a $200ms$ current injection of 50 or $90pA$. The stimulation protocol was as follows: $50ms$ prerun without stimulation, followed by $200ms$ somatic current injection of 50 or $90pA$ followed by a $50ms$ long period without current injection.

We extracted the following 9 spiking properties (**Figures 1A**) from the raw traces of current injections with 50 and $90pA$:

1. Numbers of spikes fired within $200ms$ under current clamp.
2. Latency of first spike after stimulus onset in ms.

3. The voltage threshold was defined as the voltage at which the rate of change of membrane potential exceeded $15\frac{mV}{ms}$.
4. Average amplitude of spikes.
5. The fast after hyperpolarisation (fAHP) amplitude was calculated as the voltage difference between the spiking threshold and the minimum potential within $5ms$ after a spike.
6. Absolute value of fast after hyperpolarisation (fAHP) amplitude.
7. The action potential width was measured at half the height of the spike amplitude.
8. Interspike interval (ISI) in ms between the first and second spike during current clamp.
9. The adaptation index AI was calculated in the following manner: $AI = 1 - \frac{ISI_1}{ISI_{end}}$, where ISI_1 is the first and ISI_{end} the last ISI.

The spiking features for any given parameter combination in the model were then compared with the same experimentally derived spiking features (Mongiat *et al.*, 2009) and expressed in units of standard deviation. This approach allowed us to take into account the intrinsic variability of each feature separately. The overall fitness F_i of spike feature i was defined as:

$$F_i = \frac{|SF_i - \overline{SF}_{i,exp}|}{SD_{i,exp}} \tag{1}$$

where $\overline{SF}_{i,exp}$ refers to the average value of the spike feature i and $SD_{i,exp}$ to the standard deviation of the spike feature i across all recorded GCs. The value of the spike feature of the corresponding model for a given parameter combination was SF_i. For a parameter combination to be accepted as a valid combination, it was required to fulfil the following condition:

$$P = max\left(\frac{|SF_i - \overline{SF}_{i,exp}|}{SD_{i,exp}}\right) < 2,\ for\ i = 1, 2, ..., 9 \quad (2)$$

The value of the Pareto efficiency P corresponded to the fitness F_i of the spiking feature SF_i that deviated most from the experimental average.

The search algorithm

To search for parameter sets that match our criteria for valid GC activity we combined random sampling with a gradient descent algorithm. In order to search for local minima we used a conjugate gradient descent technique (Press *et al.*, 2007). Conjugate gradient descent techniques involve successive calculations of local gradients followed by the exploration of the parameter space along a vector derived from that gradient. Starting from a random or given point in the parameter space, we calculated the gradients for each dimension with two sample points to smooth the slopes. The algorithm evaluates the calculated gradients of the fitness function in each dimension and moves in the direction of the steepest descent with respect to the cost function. The sample points where calculated in steps of $\pm 5\%$ of the corresponding parameter value. This procedure was then repeated until the method converged to a local minimum of the corresponding Pareto efficiency P (**Equation 2**). The successive line minimisation was done in conjugated directions, so that the successive minimisations were as independent as possible. Theoretically, this ensured that the parameter search found a local minimum of the target function P. For some initial parameter combinations, large areas of the parameter space were completely flat (i.e. the gradient was zero). This was especially the case when the initial models showed no spiking activity (**Figure S2B**). In this case, we increased the size of the iteration steps consecutively by $\pm 5\%$. If still (after increasing the step size to $\pm 50\%$) no gradients other than zero were found or the local minima did not fulfil the criteria of functional GC excitability, we randomised the parameters in the next step in an iteratively increasing range (from $\pm 10\%$ of

the corresponding parameter values in steps of $\pm 10\%$ up to $\pm 50\%$). The gradient descent algorithm was used to find the parameter settings of the reduced models. Starting from the full model (**Figure 1C**, **Table S1, S2 and S3**), we gradually reduced the number of ion channels, starting with the channels that influenced the cost function the least.

Diversity expansion

In order to generate models with controllable amounts of ion channels we used the reduced $5-$channel model as a basis. We then produced multiple instances each of the remaining potassium (BK) and calcium (Cav22) channels. Each artificial channel form obtained in such a way was associated with a randomised time constant between $0\times$ and $2\times$ the value in the original GC model to obtain altered dynamics. Furthermore, we randomised the conductances and applied the search algorithm to reproduce characteristic GC activity to derive all base models with different complexities in **Figure 4**.

Toy model

We created a toy model to test whether the law of large numbers is a plausible explanation for the phenomena we observed in the GC model. In order to mimic the distribution of functional overlapping ion channel expressions in a population of GC models around a genetically targeted functional set point we used randomly uniformly sampled variables between zero and two (**Figure 3D**). A valid toy model is defined as having a smaller average deviation from the mean (targeted value) than 0.015. By decreasing the sample range around the mean in steps of 0.1 down to a sample range between 0.9 and 1.1 we change the intensity of fluctuations around the target point (**Figure 3D**).

To expand the toy model to account for possible intrinsic correlations in the expres-

sion of ion channels (**Figure S6**), we used a Gaussian copula to impose a correlation structure on the random variables with uniform marginals and specified pairwise correlations. For a desired positive pairwise correlation ρ in a system of n variables we generated an $n \times n$ correlation matrix $\mathbf{R}$ with elements $\mathbf{R}_{i,j} = \rho$ if $i \neq j$ and $\mathbf{R}_{i,i} = 1$. If a random variable $\mathbf{u} = (u_1, u_2, ..., u_n)$ and each u_i is independently uniformly distributed in the range $[0, 1]$, then the correlated random variable $\mathbf{v}$ with uniform marginals on $[0, 1]$ is given by

$$\mathbf{v} = \mathbf{\Phi}_{\mathbf{R}}\big(\Phi^{-1}(u_1), \Phi^{-1}(u_2), ..., \Phi^{-1}(u_n)\big) \tag{3}$$

where $\mathbf{\Phi}_{\mathbf{R}}$ is the cumulative distribution function of a multivariate Gaussian distribution in n-dimensions with mean 0 and covariance matrix $\mathbf{R}$ and Φ^{-1} is the inverse cumulative distribution function of a standard univariate Gaussian. Multiplying $\mathbf{v}$ by 2 maps it back to the same space as the uncorrelated toy model.

Hyperplanes

To learn more about the relationship of the set of valid models, we created linear combinations of our best solutions. This method was adopted from Achard and De Schutter (2006) and allowed us to better estimate whether the solutions lie on a common low-dimensional manifold within the high-dimensional parameter space of the GC model variants (**Figure S7 – S9**). As a first step, we created linear combinations out of weighted sums of a pair of solutions. We weighted the parameters of the respective model between 0.1 and 0.9 with a step size of 0.1. The weighting of the second solution was chosen such that the sum of the weights was equal to 1. As soon as the Pareto efficiency of all evaluated linear combinations fulfilled the criteria for characteristic GC spiking, we assumed that the respective models were connected. In the next step, we created linear combinations of three different valid solutions to visualise the hyperplanes in two dimensions. We used several triplets of valid parameter sets and weighted two of them with values between -1.5 and 2.5 using a step size of 0.04. The corresponding grid of

combinations was visualised in a two-dimensional plot. The weighting of the third selected parameter set was chosen in a way that the sum of all weights was equal to 1. The hyperplanes consisted of several thousand points, whereby the parameter sets with negative values were removed. As a result, each hyperplane had different boundaries and thus a different size. Finally, for each of these points we ran simulations and calculated their Pareto efficiency. The Pareto efficiency of the models without spiking behaviour was set to 6, which explains the abrupt change of colour on the right side of **Figure S7**. The colour selection of the plots allowed a clear distinction between the valid (green) and the nonvalid (blue) models.

References

Abbott LF, LeMasson G (1993) Analysis of neuron models with dynamically regulated conductances. *Neural Computation* 5:823–842.

Achard P, De Schutter E (2006) Complex parameter landscape for a complex neuron model. *PLoS Computational Biology* 2:e94.

Aizenman CD, Akerman CJ, Jensen KR, Cline HT (2003) Visually driven regulation of intrinsic neuronal excitability improves stimulus detection in vivo. *Neuron* 39:831–842.

Alonso LM, Marder E (2019) Visualization of currents in neural models with similar behavior and different conductance densities. *eLife* 8:e42722.

Bahl A, Stemmler MB, Herz AV, Roth A (2012) Automated optimization of a reduced layer 5 pyramidal cell model based on experimental data. *Journal of Neuroscience Methods* 210:22–34.

Bean BP (2007) The action potential in mammalian central neurons. *Nature Reviews Neuroscience* 8:451–465.

Beining M, Mongiat LA, Schwarzacher SW, Cuntz H, Jedlicka P (2017) T2N as a new tool for robust electrophysiological modeling demonstrated for mature and adult-born dentate granule cells. *eLife* 6:e26517.

Britton OJ, Bueno-Orovio A, Van Ammel K, Lu HR, Towart R, Gallacher DJ, Rodriguez B (2013) Experimentally calibrated population of models predicts and explains intersubject variability in cardiac cellular electrophysiology. *PNAS* 110:E2098–E2105.

Coetzee WA, Amarillo Y, Chiu J, Chow A, Lau D, Mccormack T, Morena H, Nadal MS, Ozaita A, Pountney D, Saganich M, Miera EVS, Rudy B (2006) Molecular diversity of K+ channels. *Annals of the New York Academy of Sciences* 868:233–255.

Connors BW, Gutnick MJ (1990) Intrinsic firing patterns of diverse neocortical neurons. *Trends in Neurosciences* 13:99–104.

Cuntz H, Bird AD, Mittag M, Beining M, Schneider M, Mediavilla L, Hoffmann FZ, Deller T, Jedlicka P (2021) A general principle of dendritic constancy: A neuron's size- and shape-invariant excitability. *Neuron* 109:3647–3662.e7.

Cuntz H, Forstner F, Borst A, Häusser M (2010) One rule to grow them all: A general theory of neuronal branching and its practical application. *PLoS Computational Biology* 6:e1000877.

Cuntz H, Forstner F, Borst A, Häusser M (2011) The TREES Toolbox—Probing the basis of axonal and dendritic Branching. *Neuroinformatics* 9:91–96.

Drion G, O'Leary T, Marder E (2015) Ion channel degeneracy enables robust and tunable neuronal firing rates. *PNAS* 112:E5361–E5370.

Druckmann S (2007) A novel multiple objective optimization framework for constraining conductance-based neuron models by experimental data. *Frontiers in Neuroscience* 1:7–18.

Edelman GM, Gally JA (2001) Degeneracy and complexity in biological systems. *PNAS* 98:13763–13768.

Franci A, O'Leary T, Golowasch J (2020) Positive dynamical networks in neuronal regulation: How tunable variability coexists with robustness. *IEEE Control Systems Letters* 4:946–951.

Fujita H, Kodama T, Du Lac S (2020) Modular output circuits of the fastigial nucleus for diverse motor and nonmotor functions of the cerebellar vermis. *Elife* 9:e58613.

Gal A, Eytan D, Wallach A, Sandler M, Schiller J, Marom S (2010) Dynamics of excitability over extended timescales in cultured cortical neurons. *Journal of Neuroscience* 30:16332–16342.

Gjorgjieva J, Drion G, Marder E (2016) Computational implications of biophysical diversity and multiple timescales in neurons and synapses for circuit performance. *Current Opinion in Neurobiology* 37:44–52.

Goaillard JM, Marder E (2021) Ion channel degeneracy, variability, and covariation in neuron and circuit resilience. *Annual Review of Neuroscience* Online ahead of print.

Golowasch J, Marder E (1992) Ionic currents of the lateral pyloric neuron of the stomatogastric ganglion of the crab. *Journal of Neurophysiology* 67:318–331.

Golowasch J, Casey M, Abbott LF, Marder E (1999) Network stability from activity-dependent regulation of neuronal conductances. *Neural Computation* 11:1079–1096.

Golowasch J, Goldman MS, Abbott LF, Marder E (2002) Failure of averaging in the construction of a conductance-based neuron model. *Journal of Neurophysiology* 87:1129–1131.

Gunay C, Edgerton JR, Jaeger D (2008) Channel density distributions explain spiking variability in the globus pallidus: A combined physiology and computer simulation database approach. *Journal of Neuroscience* 28:7476–7491.

Guo W, Jung WE, Marionneau C, Aimond F, Xu H, Yamada KA, Schwarz TL, Demolombe S, Nerbonne JM (2005) Targeted deletion of Kv4.2 eliminates Ito,f and

results in electrical and molecular remodeling, with no evidence of ventricular hypertrophy or myocardial dysfunction. *Circulation Research* 97:1342–1350.

Hay E, Hill S, Schürmann F, Markram H, Segev I (2011) Models of neocortical layer 5b pyramidal cells capturing a wide range of dendritic and perisomatic active properties. *PLoS Computational Biology* 7:e1002107.

Herrera-Valdez MA, McKiernan EC, Berger SD, Ryglewski S, Duch C, Crook S (2013) Relating ion channel expression, bifurcation structure, and diverse firing patterns in a model of an identified motor neuron. *Journal of Computational Neuroscience* 34:211–229.

Hille B (2001) *Ion channels of excitable membranes* Oxford University Press.

Hines ML, Carnevale NT (1997) The NEURON simulation environment. *Neural Computation* 9:1179–1209.

Iacobas DA, Iacobas S, Lee PR, Cohen JE, Fields RD (2019) Coordinated activity of transcriptional networks responding to the pattern of action potential firing in neurons. *Genes* 10:754.

Jarsky T, Roxin A, Kath WL, Spruston N (2005) Conditional dendritic spike propagation following distal synaptic activation of hippocampal CA1 pyramidal neurons. *Nature Neuroscience* 8:1667–1676.

Jedlicka P, Bird AD, Cuntz H (2022) Pareto optimality, economy–effectiveness trade-offs and ion channel degeneracy: improving population modelling for single neurons. *Open Biology* 12:14–23.

Keren N, Peled N, Korngreen A (2005) Constraining compartmental models using multiple voltage recordings and genetic algorithms. *Journal of Neurophysiology* 94:3730–3742.

Khorkova O, Golowasch J (2007) Neuromodulators, not activity, control coordinated expression of ionic currents. *Journal of Neuroscience* 27:8709–8718.

Kirkpatrick S, Gelatt CD, Vecchi MP (1983) Optimization by simulated annealing. *Science* 220:671–680.

Kodama T, Gittis AH, Shin M, Kelleher K, Kolkman KE, McElvain L, Lam M, Du Lac S (2020) Graded coexpression of ion channel, neurofilament, and synaptic genes in fast-spiking vestibular nucleus neurons. *Journal of Neuroscience* 40:496–508.

Liu Z, Golowasch J, Marder E, Abbott LF (1998) A model neuron with activity-dependent conductances regulated by multiple calcium sensors. *Journal of Neuroscience* 18:2309–2320.

MacLean JN, Zhang Y, Goeritz ML, Casey R, Oliva R, Guckenheimer J, Harris-Warrick RM (2005) Activity-independent coregulation of IA and Ih in rhythmically active neurons. *Journal of Neurophysiology* 94:3601–3617.

MacLean JN, Zhang Y, Johnson BR, Harris-Warrick RM (2003) Activity-independent homeostasis in rhythmically active neurons. *Neuron* 37:109–120.

Marder E (2011) Variability, compensation, and modulation in neurons and circuits. *PNAS* 108:15542–15548.

Marder E, Goaillard JM (2006) Variability, compensation and homeostasis in neuron and network function. *Nature Reviews Neuroscience* 7:563–574.

Marder E, O'Leary T, Shruti S (2014) Neuromodulation of circuits with variable parameters: single neurons and small circuits reveal principles of state-dependent and robust neuromodulation. *Annual Review of Neuroscience* 37:329–346.

Mishra P, Narayanan R (2021) Ion-channel regulation of response decorrelation in a heterogeneous multi-scale model of the dentate gyrus. *Current Research in Neurobiology* 2:100007.

Mitchell M (1998) *An Introduction to Genetic Algorithms* MIT Press.

Mongiat LA, Espósito MS, Lombardi G, Schinder AF (2009) Reliable activation of immature neurons in the adult hippocampus. *PLoS One* 4:e5320.

Nerbonne JM, Gerber BR, Norris A, Burkhalter A (2008) Electrical remodelling maintains firing properties in cortical pyramidal neurons lacking KCND2-encoded A-type K+ currents. *Journal of Physiology* 586:1565–1579.

O'Leary T, van Rossum MC, Wyllie DJ (2010) Homeostasis of intrinsic excitability in hippocampal neurones: Dynamics and mechanism of the response to chronic depolarization. *Journal of Physiology* 588:157–170.

O'Leary T, Williams AH, Caplan JS, Marder E (2013) Correlations in ion channel expression emerge from homeostatic tuning rules. *PNAS* 110:E2645–E2654.

O'Leary T, Williams AH, Franci A, Marder E (2014) Cell types, network homeostasis, and pathological compensation from a biologically plausible ion channel expression model. *Neuron* 82:809–821.

Olypher AV, Calabrese RL (2007) Using constraints on neuronal activity to reveal compensatory changes in neuronal parameters. *Journal of Neurophysiology* 98:3749–3758.

Pallasdies F, Norton P, Schleimer JH, Schreiber S (2021) Neural optimization: Understanding trade-offs with pareto theory. *Current Opinion in Neurobiology* 71:84–91.

Press WH, Teukolsky SA, Vetterling WT, Flannery BP (2007) *Numerical Recipes* Cambridge University Press.

Prinz AA, Billimoria CP, Marder E (2003) Alternative to hand-tuning conductance-based models: construction and analysis of databases of model neurons. *Journal of Neurophysiology* pp. 3998 – 4015.

Prinz AA, Bucher D, Marder E (2004) Similar network activity from disparate circuit parameters. *Nature Neuroscience* 7:1345–1352.

Raj A, van Oudenaarden A (2008) Nature, nurture, or chance: stochastic gene expression and its consequences. *Cell* 135:216–226.

Rathour RK, Narayanan R (2019) Degeneracy in hippocampal physiology and plasticity. *Hippocampus* 29:980–1022.

Rudy B (1988) Diversity and ubiquity of K channels. *Neuroscience* 25:729–749.

Schmidt-Hieber C, Jonas P, Bischofberger J (2007) Subthreshold dendritic signal processing and coincidence detection in dentate gyrus granule cells. *Journal of Neuroscience* 27:8430–8441.

Schulz DJ, Goaillard JM, Marder E (2007) Quantitative expression profiling of identified neurons reveals cell-specific constraints on highly variable levels of gene expression. *PNAS* 104:13187–13191.

Schulz DJ, Goaillard JM, Marder E (2006) Variable channel expression in identified single and electrically coupled neurons in different animals. *Nature Neuroscience* 9:356–362.

Sekulic V, Lawrence JJ, Skinner FK (2014) Using multi-compartment ensemble modeling as an investigative tool of spatially distributed biophysical balances: Application to hippocampal oriens-lacunosum/moleculare (O-LM) cells. *PLoS ONE* 9:e106567.

Sigal A, Milo R, Cohen A, Geva-Zatorsky N, Klein Y, Liron Y, Rosenfeld N, Danon T, Perzov N, Alon U (2006) Variability and memory of protein levels in human cells. *Nature* 444:643–646.

Stegen M, Kirchheim F, Hanuschkin A, Staszewski O, Veh RW, Wolfart J (2012) Adaptive intrinsic plasticity in human dentate gyrus granule cells during temporal lobe epilepsy. *Cerebral Cortex* 22:2087–2101.

Swensen AM (2005) Robustness of burst firing in dissociated Purkinje neurons with acute or long-term reductions in sodium conductance. *Journal of Neuroscience* 25:3509–3520.

Tapia M, Baudot P, Formisano-Tréziny C, Dufour MA, Temporal S, Lasserre M, Marquèze-Pouey B, Gabert J, Kobayashi K, Goaillard JM (2018) Neurotransmitter

identity and electrophysiological phenotype are genetically coupled in midbrain dopaminergic neurons. *Scientific reports* 8:1–14.

Tononi G, Sporns O, Edelman GM (2002) Measures of degeneracy and redundancy in biological networks. *PNAS* 96:3257–3262.

Turrigiano G, Desai NS, Rutherford LC (1999) Plasticity in the intrinsic excitability of cortical pyramidal neurons. *Nature Neuroscience* 2:515–520.

Van Geit W, De Schutter E, Achard P (2008) Automated neuron model optimization techniques: a review. *Biological cybernetics* 99:241–251.

Vanier MC, Bower JM (1999) A comparative survey of automated parameter-search methods for compartmental neural models. *Journal of Computational Neuroscience* 7:149–171.

Yang J, Shakil H, Ratté S, Prescott SA (2022) Minimal requirements for a neuron to coregulate many properties and the implications for ion channel correlations and robustness. *Elife* 11:e72875.

Young CC, Stegen M, Bernard R, Müller M, Bischofberger J, Veh RW, Haas CA, Wolfart J (2009) Upregulation of inward rectifier K+ (Kir2) channels in dentate gyrus granule cells in temporal lobe epilepsy. *Journal of Physiology* 587:4213–4233.

Zhang Y, Oliva R, Gisselmann G, Hatt H, Guckenheimer J, Harris-Warrick RM (2003) Overexpression of a hyperpolarization-activated cation current (Ih) channel gene modifies the firing activity of identified motor neurons in a small neural network. *Journal of Neuroscience* 23:9059–9067.

Supporting information

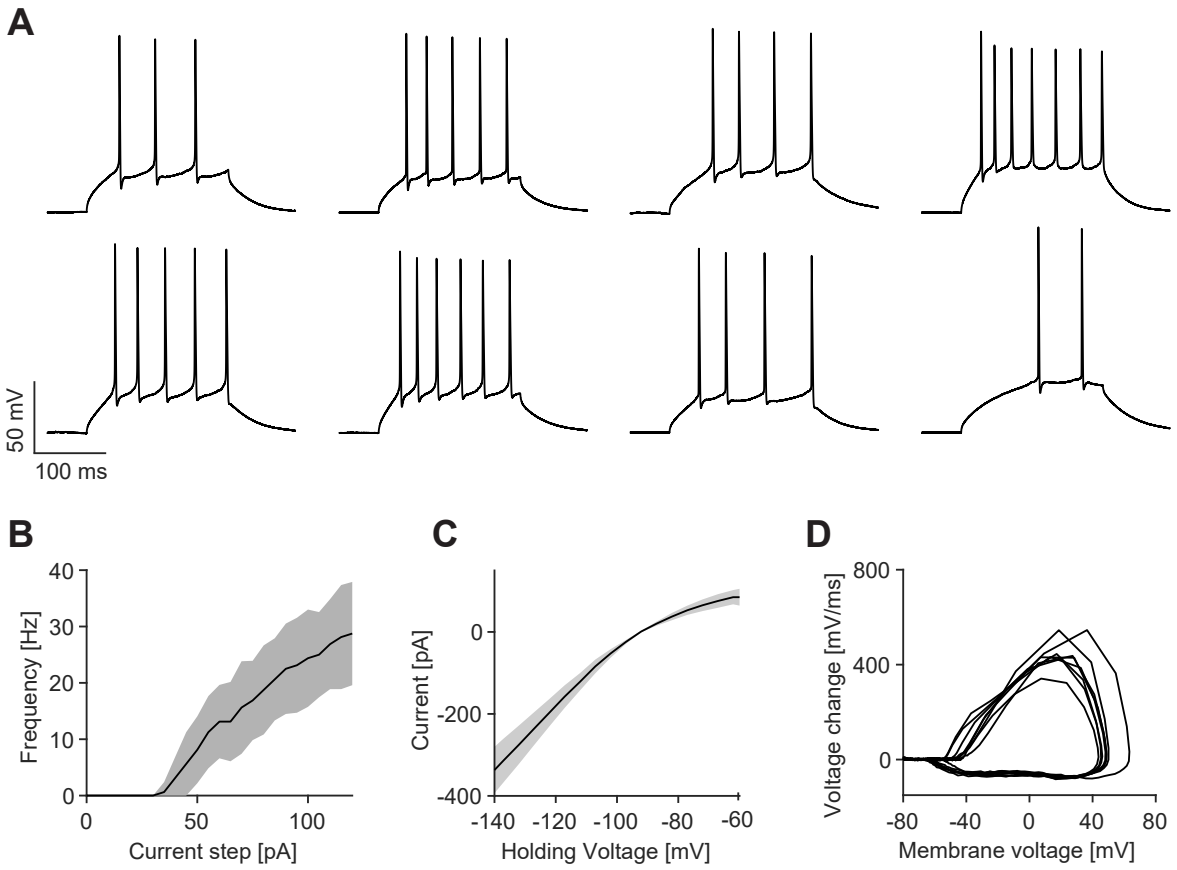

Figure S1. Electrophysiological properties of mouse GCs.

Experimental data from (Mongiat *et al.*, 2009). **A**, Voltage traces of eight different GCs during $200ms$ current clamp injection of $90pA$. **B**, Frequency of action potentials elicited by $200ms$ lasting current injections (mean and standard deviation from raw traces, experimental standard deviation is shown as grey patches). **C**, Current-voltage (I–V) relationships (mean and standard deviation from raw traces, experimental standard deviation is shown as grey patches). **D**, Phase plots of the first action potential during $90pA$ current clamp. Modified from Figure 2 in Beining *et al.* (2017).

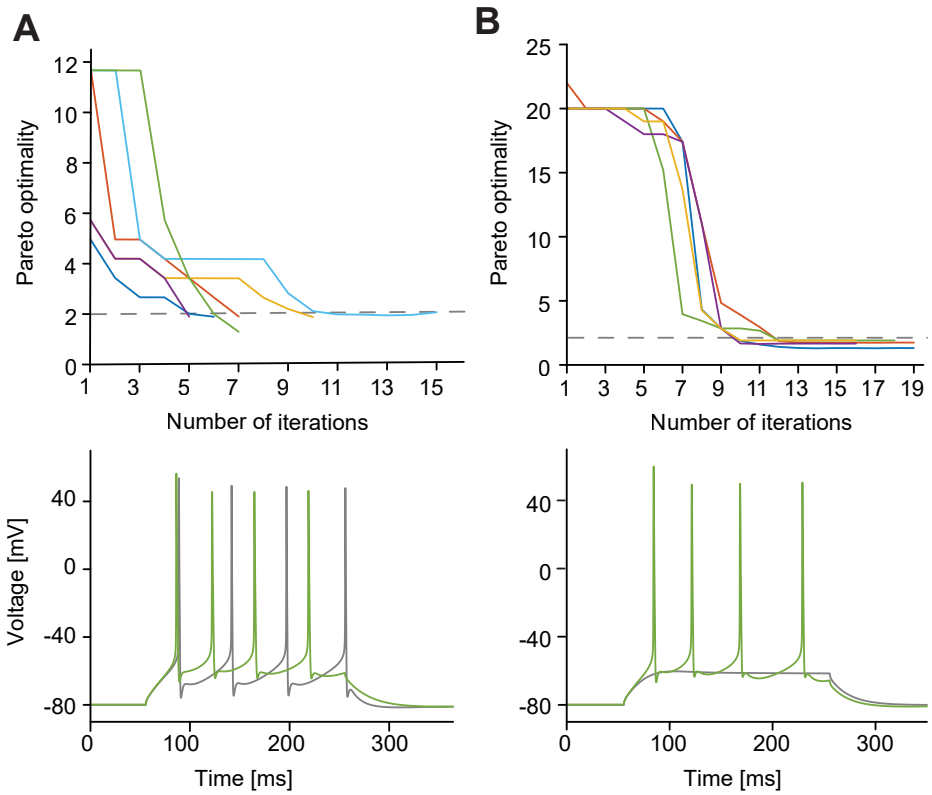

Figure S2. Gradient descent using multi-objective optimisation.

A, Temporal evolution of Pareto optimality (*top*, see Eq. 2) using the gradient descent method. Solutions are considered valid once their Pareto optimality drops below 2 (dashed line). Initial parameter combinations are random non-valid parameter combinations within a range between $0\times$ and $2\times$ the value in the reference parameter set. (*bottom*) Voltage traces of the model with initial parameter combinations (grey) and optimised parameters (green). **B**, Same as in **A**, but all initial parameter combinations were in a similar order of magnitude of Pareto optimality with corresponding models that did not even produce spikes.

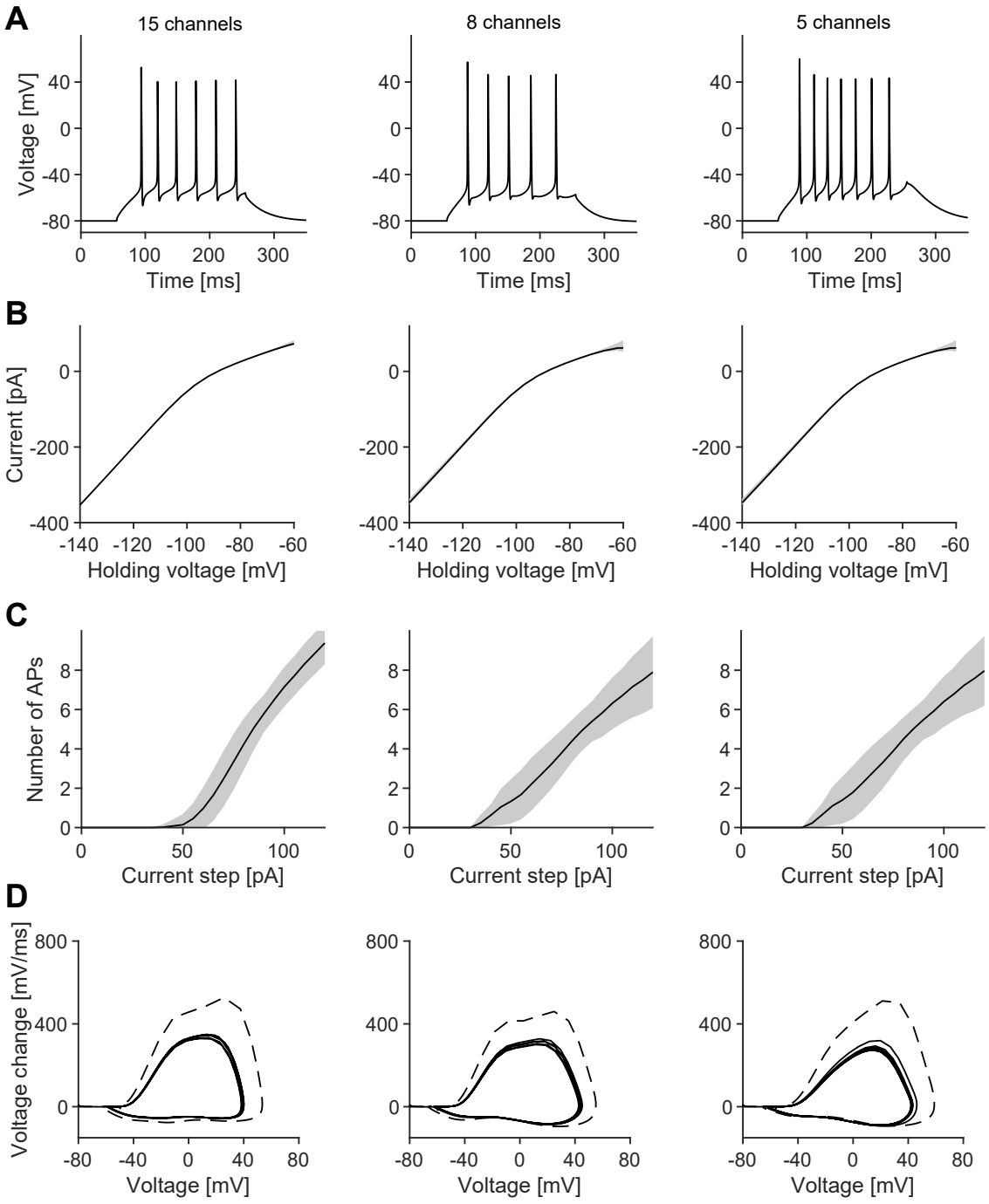

Figure S3. Comparison of the different GC models in Figure 1C.

A–D, Similar panels as in **Figure S1** for the different models and respective parameter combinations as in **Figure 2A**.

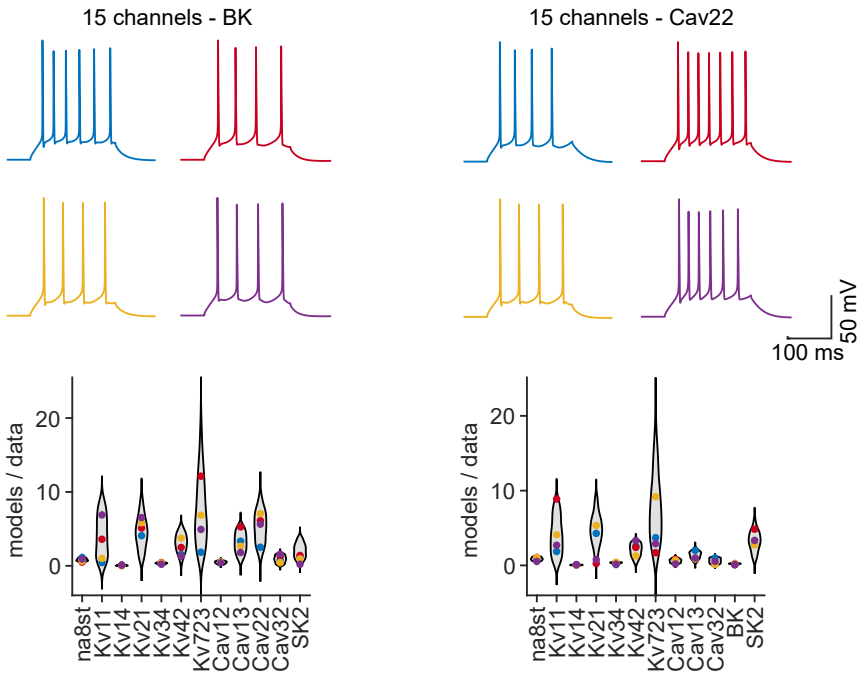

Figure S4. Valid parameter combinations in models that compensate for the knock-out of the BK (Left) and Cav22 (Right) channel.

Valid parameter combinations in the fully complex model are well spread and more stable as compared to reduced models. Activity traces of 4 randomly picked valid parameter combinations in models successfully compensating the corresponding knock-out (Top). Coloured dots illustrate conductance densities of the four valid parameter combinations shown in top traces (Bottom). Violin plots show the probability distribution of valid parameter combinations. Conductances are weighted by the surface area of the corresponding membrane regions.

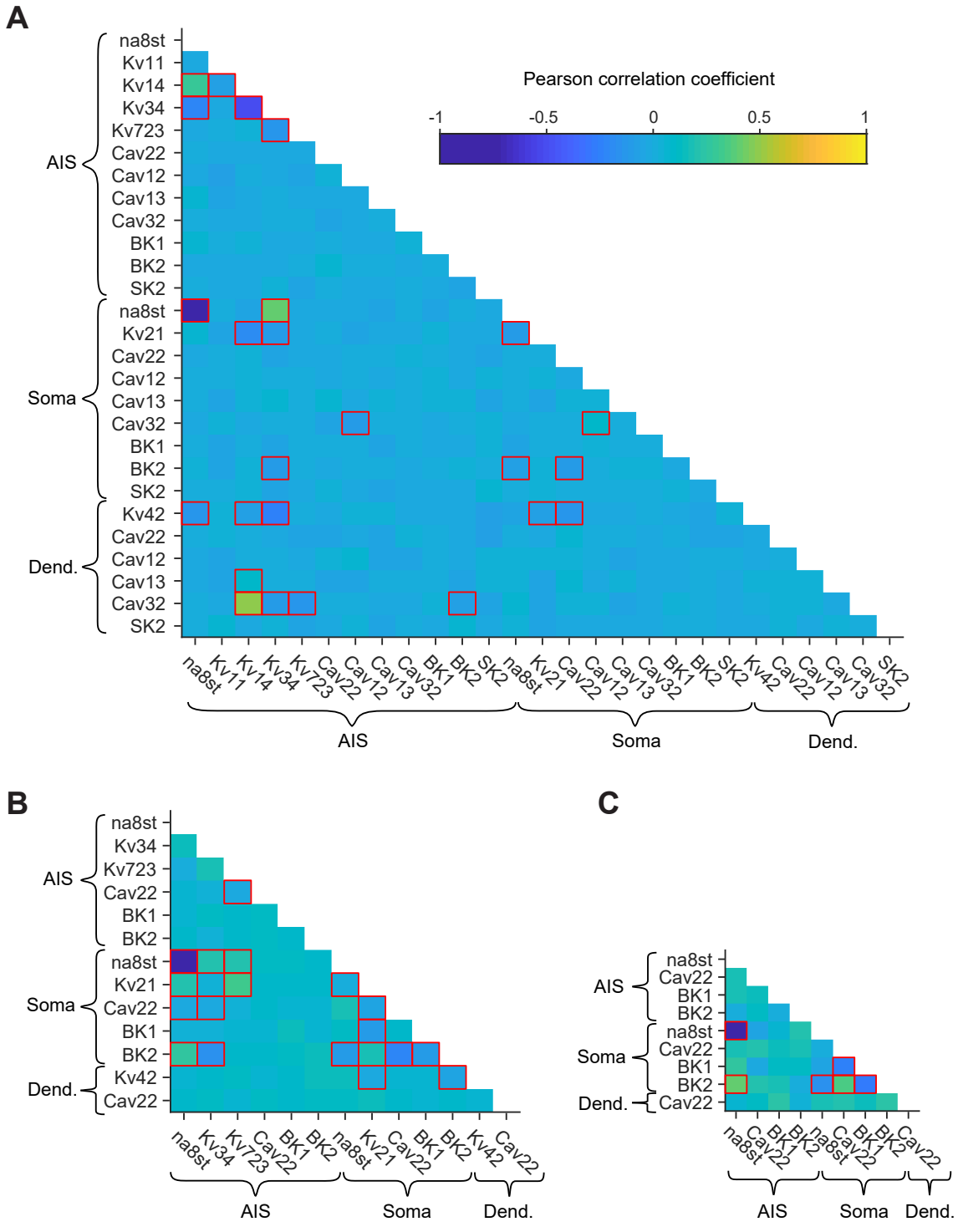

Figure S5. Correlations between pairs of channel conductances in the different populations. Significant correlations are highlighted by red boxes (p-value < 0.01). Pairwise correlations in population of **A**, $15-$channel models, **B**, $9-$channel models, **C**, $5-$channel models.

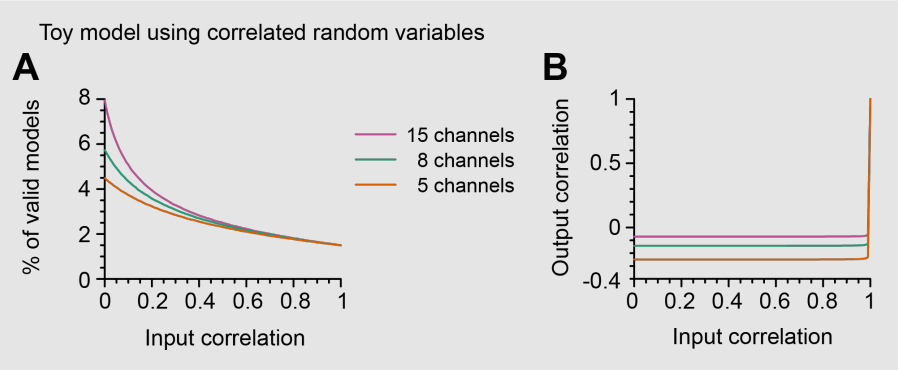

Figure S6. Correlations in the toy model.

A, Effects of pairwise correlations on the proportion of valid models for different numbers of variables. The 1 variable model is not plotted as it is not affected by correlations. All models converge to the same point as their elements become perfectly correlated and the effective number of dimensions is reduced to 1. **B**, Observed output correlations in valid models as a function of the pairwise correlation used to generate the population from which valid models are drawn. For almost all input correlations the observed correlation depends only on the number of variables.

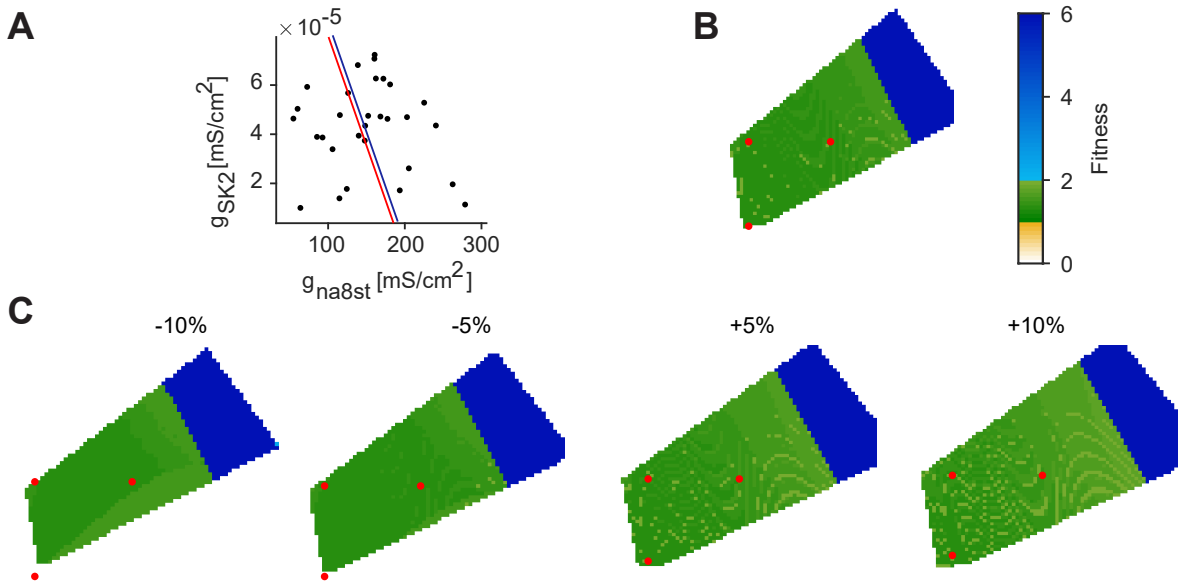

Figure S7. 2D illustrations of hyperplanes in the parameter space.

Hyperplane analysis inspired by Achard and De Schutter (2006) for the $15-$channel model. **A**, The hyperplane of **B** is shown in red as projection onto $g_{Na8st,AIS}$ vs. $g_{SK2,AIS}$ plane. 25 randomly chosen valid parameter combinations are represented by dots. The blue hyperplane is parallel to the red and is defined by the addition of 10% of the SD of all solutions (in every dimension). **B**, Hyperplane defined by the three individuals on the red line in **A**. The Fitness of all points is colour scaled. The three original individuals are highlighted as red dots. **C**, The red dots mark the places parallel to the 3 originally selected individuals.

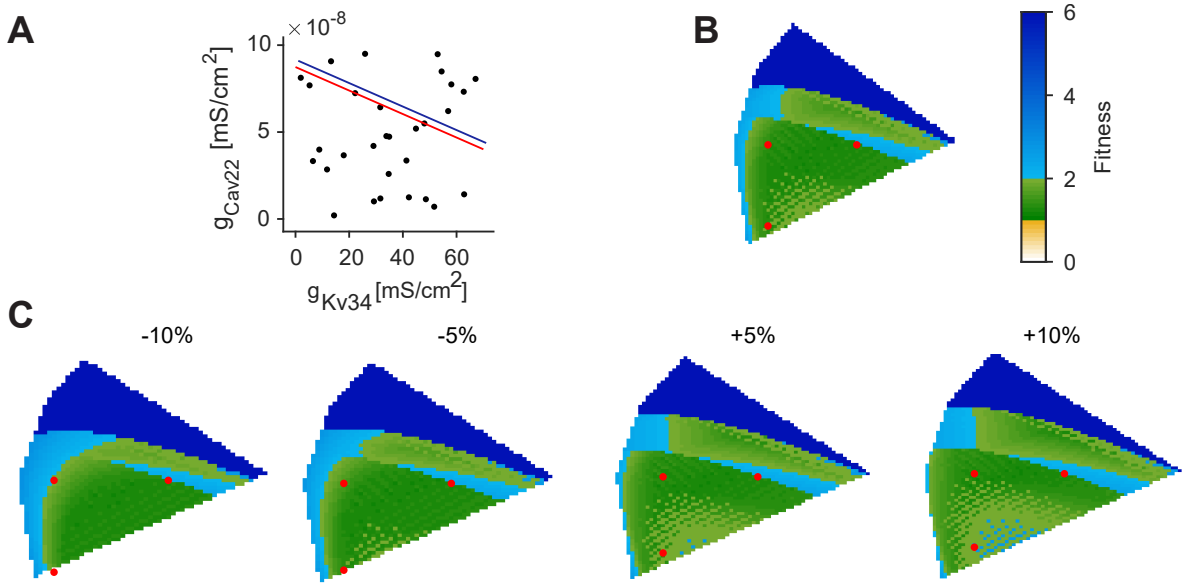

Figure S8. 2D illustrations of hyperplanes in the parameter space.

Hyperplane analysis inspired by Achard and De Schutter (2006) for the $9-$channel model. **A**, The hyperplane of **B** is shown in red as projection onto $g_{Kv34,AIS}$ vs. $g_{Cav22,AIS}$ plane. 25 randomly chosen valid parameter combinations are represented by dots. The blue hyperplane is parallel to the red and is defined by the addition of 10% of the SD of all solutions (in every dimension). **B**, Hyperplane defined by the three individuals on the red line in **A**. The Fitness of all points is colour scaled. The three original individuals are highlighted as red dots. **C**, The red dots mark the places parallel to the 3 originally selected individuals.

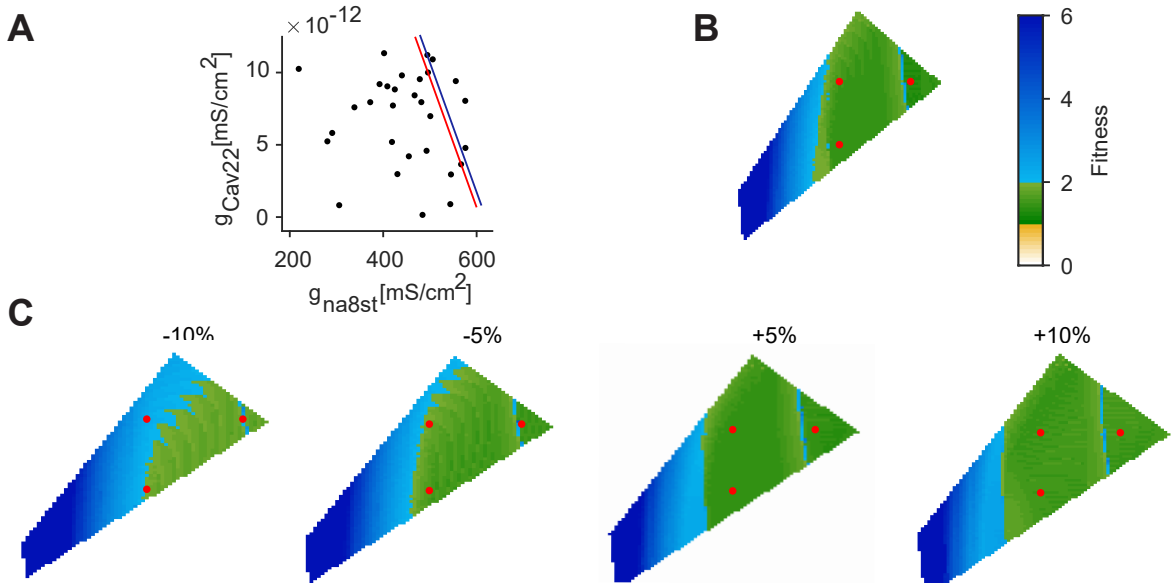

Figure S9. 2D illustrations of hyperplanes in the parameter space.

Hyperplane analysis inspired by Achard and De Schutter (2006) for the $5-$channel model. **A**, The hyperplane of **B** is shown in red as projection onto $g_{na8st,AIS}$ vs. $g_{Cav22,AIS}$ plane. 25 randomly chosen valid parameter combinations are represented by dots. The blue hyperplane is parallel to the red and is defined by the addition of 10% of the SD of all solutions (in every dimension). **B**, Hyperplane defined by the three individuals on the red line in **A**. The Fitness of all points is colour scaled. The three original individuals are highlighted as red dots. **C**, The red dots mark the places parallel to the 3 originally selected individuals.

Name	AIS	Soma	Dendrite
pas	6.593×10^{-6}	1.385×10^{-5}	1.385×10^{-5}
Kir 2.1	6.741×10^{-5}	1.415×10^{-4}	1.415×10^{-4}
Na8st	0.614	0.1478	
Kv 1.1	2.76×10^{-4}		
Kv 1.4	1.77×10^{-2}		
Kv 2.1		0.0022	
Kv 3.4	0.6987		
Kv 4.2			0.0039
Kv 7.2/3	0.0031		
Cav 1.2	3.1×10^{-4}	7.1×10^{-5}	2×10^{-5}
Cav 1.3	5.48×10^{-6}	2.5×10^{-5}	3.7×10^{-6}
Cav 2.2	3.19×10^{-7}	7.4×10^{-5}	5.8×10^{-6}
Cav 3.2	1.22×10^{-5}	1.6×10^{-5}	3.8×10^{-5}
BK			
α	0.0018	9.3×10^{-4}	
β	0.51	0.0148	
SK2	1.1×10^{-5}	3.7×10^{-8}	8.5×10^{-7}

Table S1. Summary of ion channel densities and models implemented in the $15-$channel model.

Ion channels and their expression profiles in the corresponding morphological compartments. Conductance densities are given in units of $^{mS}/_{cm^2}$.

Name	AIS	Soma	Dendrite
pas	6.593×10^{-6}	1.385×10^{-5}	1.385×10^{-5}
Kir 2.1	6.741×10^{-5}	1.415×10^{-4}	1.415×10^{-4}
Na8st	0.4925	0.0881	
Kv 2.1		0.0071	
Kv 3.4	0.0339		
Kv 7.2/3	0.0074		
Kv 4.2			0.0022
Cav 2.2	4.77×10^{-11}	4.5×10^{-4}	3.56×10^{-5}
BK			
α	1.25×10^{-7}	0.0043	
β	0.0148	0.0156	

Table S2. Summary of ion channel densities and models implemented in the $9-$channel model.

Ion channels and their expression profiles in the corresponding morphological compartments. Conductance densities are given in units of $^{mS}/_{cm^2}$.

Name	AIS	Soma	Dendrite
pas	6.593×10^{-6}	1.385×10^{-5}	1.385×10^{-5}
Kir 2.1	6.741×10^{-5}	1.415×10^{-4}	1.415×10^{-4}
Na8st	0.306	0.119	
Cav 2.2	5.82×10^{-15}	8.64×10^{-4}	1.22×10^{-4}
BK			
α	1.16×10^{-7}	0.0132	
β	1.321	0.0185	

Table S3. Summary of ion channel densities and models implemented in the $5-$channel model.

Ion channels and their expression profiles in the corresponding morphological compartments. Conductance densities are given in units of $^{mS}/_{cm^2}$.